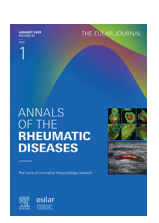


Contents lists available at ScienceDirect

Annals of the Rheumatic Diseases





Myositis

Spatial transcriptomic analysis of muscle biopsy from patients with treatment-naive juvenile dermatomyositis reveals mitochondrial abnormalities despite disease-related interferon-driven signature

Aris E. Syntakas 1,2,3, Melissa Kartawinata 1,2,3, Nia M.L. Evans 1,2,3, Huong D. Nguyen 1,2, Charalampia Papadopoulou 2,4, Muthana Al Obaidi 2,4, Clarissa Pilkington 2,4, Yvonne Glackin 4, Christopher B. Mahony 5, Adam P. Croft 5,6, Simon Eaton 2,7, Mario Cortina-Borja 2,8, Olumide Ogunbiyi 9, Ashirwad Merve 9, Lucy R. Wedderburn 1,2,3,4, Meredyth G. Ll Wilkinson 1,2,3,*, on behalf of the JDCBS

ARTICLE INFO

Article history: Received 5 February 2025 Received in revised form 14 July 2025 Accepted 15 July 2025

A B S T R A C T

Objectives: This study aimed to investigate the spatial transcriptomic landscape of muscle tissue from patients with treatment-naive juvenile dermatomyositis (JDM) in comparison to healthy paediatric muscle tissue.

Methods: Muscle biopsies from 3 patients with JDM and 3 age-matched controls were analysed using the Nanostring GeoMx Digital Spatial Profiler. Regions of interest were selected based on muscle fibres without immune cells, immune cell infiltration and CD68+ macrophage enrichment. Differential gene expression, pathway analysis and pathways clustering analysis were conducted. Key findings were validated in 19 cases of JDM using immunohistochemistry and chemical stains, and a bulk RNAseq dataset of 4 cases of JDM.

E-mail address: meredyth.wilkinson.14@ucl.ac.uk (M.G.L. Wilkinson).

Lucy R Wedderburn and Meredyth G Ll Wilkinson are joint senior authors.

Handling editor Josef S. Smolen.

https://doi.org/10.1016/j.ard.2025.07.015

¹ Infection, Immunity and Inflammation Research and Teaching Department, UCL Great Ormond Street Institute of Child Health, London, UK

 $^{^2}$ National Institute for Health and Care Research (NIHR) Biomedical Research Centre at Great Ormond Street Hospital, London, UK

³ Centre for Adolescent Rheumatology Versus Arthritis at UCL, UCL Hospital and Great Ormond Street Hospital, London, UK

⁴ Department of Rheumatology, Great Ormond Street Hospital for Children NHS Foundation Trust London, London, UK

⁵ Department of Inflammation and Ageing, School of Infection, Inflammation and Immunology, College of Medicine and Health, University of Birmingham, Birmingham, UK

⁶ NIHR Birmingham Biomedical Research Centre, Birmingham, UK

⁷ Developmental Biology and Cancer Research & Teaching Department, UCL Great Ormond Street Institute of Child Health, London, UK

⁸ Population Policy and Practice Research & Teaching Department, UCL Great Ormond Street Institute of Child Health, London, UK

⁹ Department of Histopathology, Great Ormond Street Hospital for Children NHS Foundation Trust, London, UK

^{*}Correspondence to Dr Meredyth G Ll Wilkinson, UCL GOS Institute of Child Health, and Great Ormond Street Hospital NHS Trust, University College London, London, UK.

Results: JDM muscle tissues exhibited significant interferon pathway activation and mitochondrial dysfunction compared to controls. A 15-gene interferon signature was significantly elevated in JDM muscle and macrophage-enriched regions, correlating with clinical weakness. In contrast, mitochondrial dysregulation, characterised by downregulated respiratory chain pathways, was present regardless of interferon activity or muscle strength. The interferon-driven and mitochondrial signatures were replicated in an independent RNAseq dataset from JDM muscle; the lack of association between interferon signature and mitochondrial dysregulation was validated in 19 cases by conventional staining methods. Clustering analysis revealed distinct transcriptomic profiles between JDM and control tissues, as well as between patients with JDM with varying clinical phenotypes.

Conclusions: This study highlights mitochondrial dysfunction as a consistent pathological feature in JDM muscle, which may be independent of interferon-driven inflammation. These findings highlight the potential for mitochondrial-targeted therapies in JDM management and emphasise the need for further studies to explore their therapeutic value.

WHAT IS ALREADY KNOWN ON THIS TOPIC

- Juvenile dermatomyositis (JDM) involves interferon (IFN)driven inflammation and immune-mediated muscle damage.
- Mitochondrial abnormalities in blood immune cells persist despite treatment and contribute to disease pathology.

WHAT THIS STUDY ADDS

- Mitochondrial dysfunction is present in both muscle fibres and tissue-infiltrating immune cells within JDM muscle.
- These abnormalities are detectable even in clinically less severe muscle weakness.
- Degree of mitochondrial abnormality at transcript and protein level may be independent of the strength of IFN-driven signal.
- Mitochondrial dysregulation detected at the transcriptional level correlates with abnormal transcription of muscle (sarcomere) and the subcellular peroxisome organelle.

HOW THIS STUDY MIGHT AFFECT RESEARCH, PRACTICE OR POLICY

- Targeting mitochondrial dysfunction could enhance treatment outcomes for JDM, especially in patients whose disease is refractory to current therapies.
- Insights from this study support the development of stratification tools to detect aspects of pathology which are not tightly correlated with IFN-driven pathology.

INTRODUCTION

Idiopathic inflammatory myopathies of childhood, of which the most common is juvenile dermatomyositis (JDM), are severe paediatric autoimmune conditions characterised by chronic inflammation of muscle, skin and in some cases major organs. A clear understanding of pathogenic mechanisms at the sites of tissue damage is lacking, and there is a significant unmet need for more targeted treatments [1,2]. We have previously detailed transcriptional changes detectable in blood immune cells in JDM [3]. We identified that blood CD14+ monocytes from patients with active disease have severe mitochondrial dysfunction. Furthermore, we showed that alterations in mitochondrial biology and morphology in monocytes led to accumulation of oxidised mitochondrial DNA, which was able to trigger interferon (IFN)-signalling pathways. Interestingly, while the wellcharacterised IFN-driven signature detectable at diagnosis was reduced on treatment, we observed that mitochondrial abnormalities detected in peripheral blood monocytes persisted despite treatment.

Our previous studies on JDM muscle tissue obtained before treatment showed that proinflammatory, CD68+ tissue

macrophages are frequently detectable [4,5] and that CD68+cell infiltration correlates with weakness [6]. Macrophage infiltration may be throughout the endomysium, or in perivascular clusters, where they are frequently colocalised with infiltrating T cells [5,6]. Abnormal macrophage polarisation has been implicated in perpetuating inflammation and tissue damage in myopathies [7–9]. A recent study in a myositis animal model suggests a self-perpetuating loop between mitochondrial dysfunction and inflammation [10].

To start to define at tissue level the complex interactions between immune and muscle cells in JDM-affected muscle tissue, we employed spatial transcriptomics. This method enables *in-situ* gene expression analysis while preserving critical tissue architecture, allowing precise localisation of cell types and their potential involvement in the pathogenic processes associated with myositis [11]. We employed the Nanostring GeoMx Digital Spatial Profiler (DSP) to interrogate the transcriptome of muscle tissue sections from patients with JDM and age-matched healthy controls. GeoMx facilitates the staining, selection and sequencing of specific spatial niches within the tissue known as regions of interest (ROIs) [12]. We opted to focus initially on CD68 +-enriched areas in the analysis of inflammatory infiltrate.

We confirm that JDM muscle tissue exhibits significant upregulation of IFN pathways and dysregulation of mitochondrial pathways, particularly affecting the electron transport chain. By comparing tissue areas, we show that muscle weakness correlates with increased IFN signalling in both muscleand CD68+-cell-derived transcriptome. Importantly, mitochondrial abnormalities were clearly demonstrated even in muscle with only moderate clinical weakness, and these were detected in both muscle fibres as well as in the CD68+ infiltrate. We replicated our findings in another cohort, analysing bulk RNAseq data, and validated the lack of correlation between IFN-driven changes and mitochondrial abnormality at protein level in a larger cohort. We believe that our study is the first to provide spatial transcriptional insights into JDM pathogenesis, and will facilitate significant steps towards the delineation of the contributions of immune and muscle cells, to JDM pathology. Our results suggest that mitochondrial abnormalities, which we previously defined in blood cells, are also present in both muscle and infiltrating monocyte/macrophages in JDM even before significant clinical weakness is apparent.

METHODS

All methods are provided in supplementary information.

Table
Demographics and clinical characteristics of patients with JDM and controls included in the study

| Characteristic | Value | | | | | |
|--|--------|--------|----------|------|-------|------|
| Sample ID | JDM1 | JDM2 | JDM3 | HC1 | HC2 | HC3 |
| Age at sample (y) | 5.83 | 3.58 | 4.75 | 6.28 | 10.02 | 4.81 |
| Sex | F | F | F | M | M | F |
| Disease duration at time of biopsy, months | 1.05 | 5.91 | 3.28 | NA | NA | NA |
| Myositis-specific antibody | TIF1-γ | TIF1-γ | Negative | NA | NA | NA |
| Disease activity at time of biopsy: | | | | | | |
| Physician global assess- ment score, PGA (0.0-10.0 cm) | 8.0 | 7.8 | 6.3 | NA | NA | NA |
| CMAS (0-52) | 30 | 12 | 52 | NA | NA | NA |
| MMT8 (0-80) | 44 | 42 | 78 | NA | NA | NA |
| CK, U/L | 2611 | 125 | 131 | NA | NA | NA |
| sDAS ^a | 4 | 3 | 5 | NA | NA | NA |
| Muscle biopsy score data ^b | | | | | | |
| Inflammatory domain (0-12) | 7 | 8 | 7 | NA | NA | NA |
| Muscle-fibre domain (0-10) | 8 | 7 | 7 | NA | NA | NA |
| Vascular domain (0-3) | 2 | 1 | 1 | NA | NA | NA |
| Connective tissue domain (0-2) | 1 | 2 | 1 | NA | NA | NA |
| Total biopsy score (0- 27) | 18 | 18 | 16 | NA | NA | NA |
| Histopathology visual analogue score (0.0-10.0) | 7.0 | 8.0 | 7.0 | NA | NA | NA |

CMAS, childhood myositis assessment scale; DAS, disease activity score; ID, identification; JDM, juvenile dermatomyositis; MMT8, manual muscle testing of 8 muscles; NA, not applicable; PGA, physician global assessment; sDAS, skin disease activity score.

RESULTS

Patients and controls

Clinical and demographic features of the 3 patients with JDM and controls analysed by transcriptome profiling are shown in Table [6,13]. Of note, 2 of the patients were significantly weak at the time of biopsy as assessed by the Childhood Myositis Assessment Scale (CMAS) and Manual Muscle Testing of 8 muscles (MMT8) while the third was less weak but had more severe skin disease activity. Two patients with JDM tested positive for TIF1 γ , while the third patient was negative for myositis-specific autoantibodies (MSAs). For histological analysis, a total of 19 cases were included: the 3 transcriptome-profiled patients, along with an additional 16 JDM cases (Supplementary Table S1).

Selection of ROIs for analysis of areas with or without leukocyte infiltration in JDM muscle biopsies

To determine the dominant pathways that are altered in the muscle of patients with JDM compared to healthy muscle and to test whether mitochondrial pathways are altered in muscle tissue early in JDM, we used spatial transcriptome analysis. Imaging of quadriceps muscle biopsy sections from all 6 cases was

performed on the Nanostring GeoMx scanning platform. Immunofluorescence staining was performed to enable selection of ROIs for sequencing using a nuclear marker and morphology markers laminin, CD45, and CD68, for identification of muscle fibres, leukocytes, and macrophages, respectively. For focused transcriptome analysis of infiltrating macrophages, segmentation was used, as described [12]. Figure 1A shows control muscle tissue, where no significant immune cell infiltration or inflammation is observed; Figure 1B shows JDM muscle ROI without immune cells, while Figure 1C reveals an area with substantial inflammatory infiltration (CD45+), which was not observed in the control samples. Figure 1D shows an area with infiltrating CD68+ cells within JDM muscle with Figure 1E further illustrating the 'segmented' view of CD68 + cells, allowing for transcriptomic profiling of this specific cell type. Thus, we selected 3 different ROI types for sequencing analysis: musclefibre, muscle with immune cell infiltration, and CD68-enriched, generating a total of 28 ROIs. The breakdown of the ROIs selected is shown in Supplementary Table S2.

Histological analysis of the muscle biopsy sections is presented in Supplementary Figure S1. All 3 control cases were found to have no significant pathology or inflammation, with no infiltration by CD3+ or CD68+ immune cells, confirmed by a senior histopathologist (AM) [6,14]. None of the 3 control cases had a genetic abnormality in known mitochondrial-related diseases. A representative hematoxylin and eosin (H&E)-stained section from a control case is shown in Supplementary Figure S1A. Active inflammation in a representative JDM case is demonstrated by H&E staining (Supplementary Fig S1B), CD3 (Supplementary Fig S1C), CD68 (Supplementary Fig S1D), and CD20 staining (Supplementary Fig S1E). These classical signs of JDM muscle inflammation are reflected in the biopsy scores (inflammatory domain) [6] (Table).

Principal component analysis confirms distinct transcriptomic differences between ROI types and JDM vs control tissues

Initial data quality checks were performed on the Nanostring platform, assessing tissue and sequencing quality, as well as the performance of negative control probes. None of the 28 ROIs or control probes were flagged as unsuitable for analysis. Further quality control and normalisation techniques were applied to address technical variation across data generated from ROIs. Relative log expression plots were used to visualise effects of normalisation: Supplementary Figure S2A shows unnormalised data, with Supplementary Figure S2B displaying log counts per million normalised data. This normalisation method, integrated into the voom function of the limma-voom pipeline [15], effectively centred the median expression levels of all ROIs around zero. This indicates successful removal of unwanted technical variation, enhancing comparability across samples.

We employed principal component analysis (PCA) to assess variance within the dataset, between patients, and between types of ROIs (Supplementary Fig S2C and D). Initial PCA analysis by patient revealed that all data from patients with JDM (22 ROIs) clustered into 2 clusters, with clear separation of patients with JDM from control samples (Supplementary Fig S2C). When data were labelled by ROI type, the 2 distinct clusters of data from JDM biopsies were clarified by cell type. As expected, CD68+-selected ROIs (JDM samples only) formed a separate cluster (Supplementary Fig S2D blue symbols). Interestingly, JDM muscle-only (Supplementary Fig S2D red symbols) and JDM muscle plus-immune ROIs (Supplementary Fig S2D). Note that

^a Skin disease activity score, or modified skin DAS as defined in Lam et al

^b Data generated using validated JDM muscle biopsy score tool from Varsani et al [6].

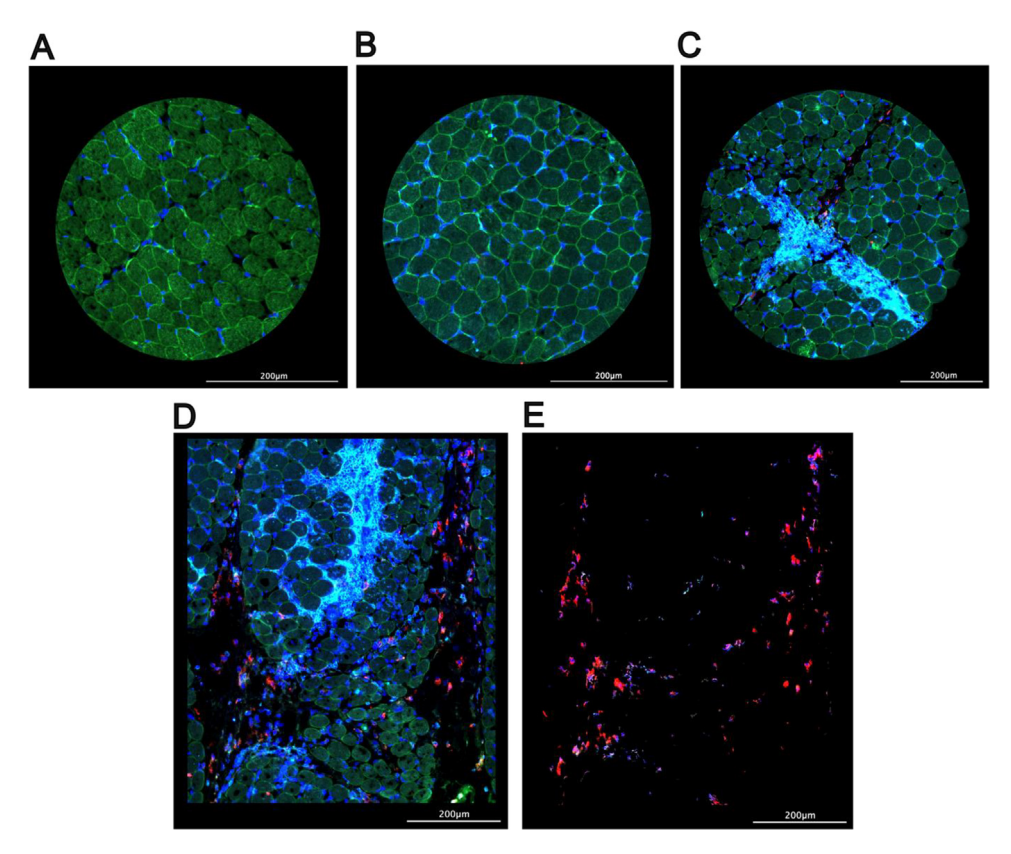


Figure 1. Immunofluorescent imaging of the muscle biopsy regions of interest (ROIs). (A-E) Representative fluorescent images of ROI types selected for sequence analysis and associated staining markers: (A) control muscle; (B) JDM muscle ROI with no infiltrating immune cells; (C) JDM muscle enriched with immune cells (CD45+); (D) CD68+ macrophage-enriched region. (E) Segmented CD68+ cells in the same region shown in (D). Staining antibodies: laminin (green), DNA nuclear stain (blue), CD68 (red), and CD45 (cyan), indicating muscle fibres, nuclei, macrophages, and leukocytes, respectively. (B-E) are derived from patient JDM3. JDM, juvenile dermatomyositis.

segmentation was not performed on CD45+ cells. Again, control muscle ROIs (Supplementary Fig S2D pink symbols) clustered away from all JDM data.

Differential gene expression analysis confirms a high IFN-driven signature and demonstrates abnormal mitochondrial gene signature in JDM muscle compared to control muscle

To investigate differences in the gene expression profiles of JDM muscle compared to control muscle, the data from muscleonly ROIs were initially used in the limma-voom differential gene expression (DGE) analysis pipeline. The analysis revealed 448 genes that were significantly differentially expressed in JDM muscle ($|Log2FC| \ge 0.58$ and adjusted P value $\le .05$, using the Benjamini-Hochberg procedure for multiple testing correction), of which 336 genes were identified as upregulated and 112 as downregulated in JDM muscle compared to control samples (Fig 2A). Pathway enrichment using over-representation analysis (ORA) on significantly differentially expressed genes (DEGs) was used to identify dysregulated pathways in JDM muscle. The gene ontology (GO) cellular component (CC) gene sets were initially used to identify differentially expressed pathways. The GO CC annotations detail the subcellular structures and complexes involved, making this appropriate for highlighting mitochondrial functional pathways. Conversely, the GO biological process (BP) gene sets were then used to capture dynamic biological activities and signalling processes, such as immune response mechanisms, which are central to JDM. The first ORA (GO CC) indicated 101 significantly differentially expressed pathways in JDM muscle compared to controls (adjusted P value

≤.05, Benjamini-Hochberg procedure) while the second (GO BP) gave 310 significant pathways.

To simplify the interpretation of these numerous, often overlapping pathways, Advanced Pathway Enrichment Analysis Representation (aPEAR) cluster network analysis was performed [16], resulting in the construction of plots that visually organise and group related pathways into coherent clusters, for each of the 2 GO gene sets that were used. The GO CC network highlighted several clusters of mitochondria-related pathways, including clusters such as the 'respiratory chain complex', the 'mitochondrial proton-transporting adenosine triphosphate (ATP) synthase complex', and the 'mitochondrial respiratory chain complex III' (Fig 2B). Interestingly, pathways related to endoplasmic reticulum (ER) to Golgi protein transport were also differentially expressed in JDM muscle (Fig 2B). The GO BP network highlighted clusters of IFN and immune-related pathways, with the most prominent clusters being 'interferon-mediated signalling pathway', 'pattern recognition receptor signalling pathway', and 'T cell mediated immunity'. In addition, several clusters related to muscle development and function were noted, including 'muscle cell development' and 'regulation of muscle contraction' (Fig 2C).

We were intrigued that a cluster of pathways annotated as 'T cell immunity' was enriched in JDM muscle-only regions (Fig 2C). Scrutiny of pathways that generated this annotation revealed 22 pathways ascribed to T cells and 85 others labelled as antigen processing, regulation of immunity, major histocompatibility complex (MHC), or other immune cells (Supplementary Table S3). Across these pathways, the top DE genes were *HLA* (human leukocyte antigen, the human MHC) genes or those involved in MHC processing such as *TAP2* (Supplementary Table

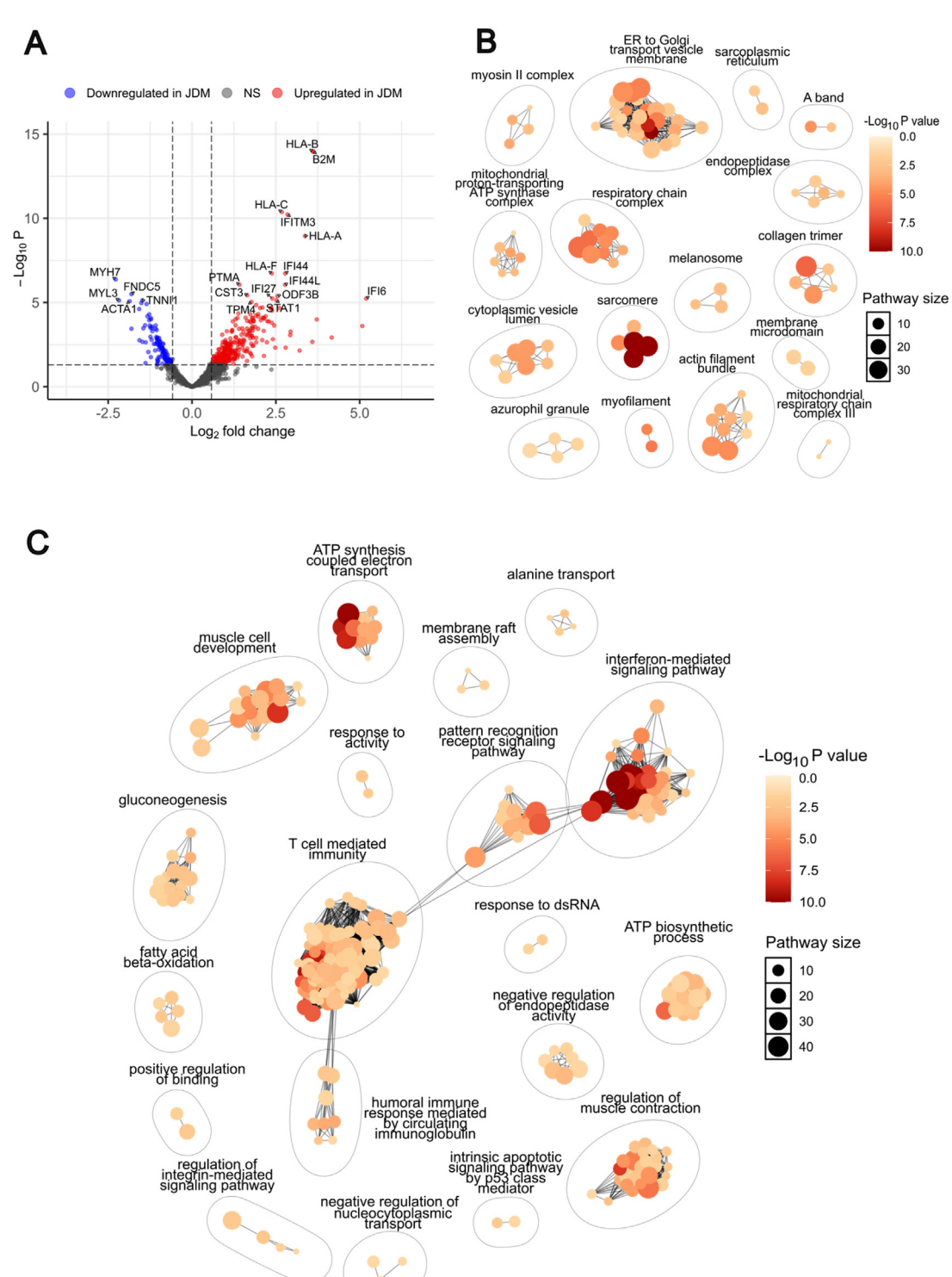


Figure 2. Differential gene expression analysis demonstrates a high interferon-driven signature and abnormal mitochondrial gene signature in JDM compared to control muscle. (A) Volcano plot illustrating differentially expressed genes (DEGs) between JDM and control muscle ROIs. Genes with an adjusted P value ≤0.05 and $|\log 2FC| \ge 0.58$ are considered statistically significant (n = 448). Red points represent significantly upregulated genes, and blue significantly downregulated genes. The 20 genes with the smallest adjusted P values were annotated. (B) Network cluster plot of enriched gene ontology cellular component (CC) pathways among the 448 DEGs, generated using the aPEAR R package. Each cluster represents groups of similar cellular components, derived from gene ontology terms. Pathways with an adjusted P value ≤0.05 (Benjamini-Hochberg procedure) were included in the clustering and network analysis. (C) Network cluster plot of enriched gene ontology biological process (BP) pathways among the 448 DEGs, generated using the aPEAR R package. Each cluster represents groups of related BPs, highlighting functional pathways involved in JDM. Pathways with an adjusted P value ≤0.05 (Benjamini-Hochberg procedure) were included in this clustering and network analysis. For (B) and (C), larger dots represent pathways associated with a higher number of significant genes (shown in key, pathway size). Dot colour intensity corresponds to significance, with deeper red shades indicating smaller P values (shown in colour bar, adjusted P value). aPEAR, advanced pathway enrichment analysis representation; FC, fold change; JDM, juvenile dermatomyositis; NS, not significant; ROI, regions of interest.

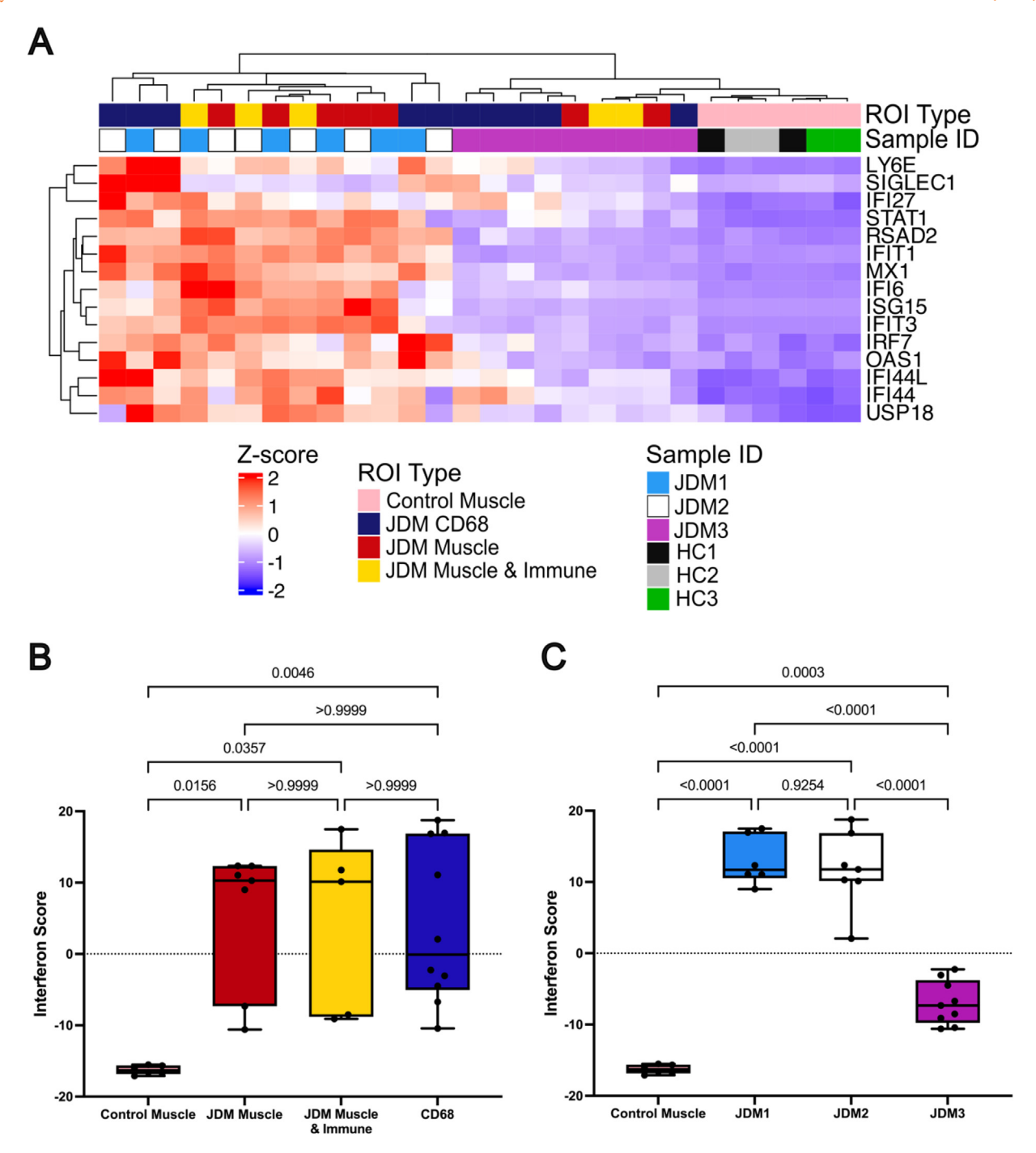


Figure 3. Interferon-driven signature is elevated across each cell type analysed in JDM tissue. (A) Heatmap showing the normalised, scaled expression levels of the 15-gene interferon score across the ROIs. Distinct ROI types (top row) are allocated colours pink, blue, red and yellow as shown; individual patients (second row sample ID) are allocated colours as shown. Unsupervised clustering groups the ROIs into 3 distinct clusters: one including ROIs patient JDM1 (light blue ID) and JDM2 (white bordered ID), a second cluster for patient JDM3 (purple ID), and a third for control ROIs (black, grey and green IDs). The coloured scaled bar red to blue highlights the *Z*-score ranges, with red indicating a positive *Z*-score and blue indicating a negative *Z*-score. (B, C) Boxplots showing the 15-gene interferon score, calculated as the sum of *Z*-scores for the 15 ISGs, compared across: (B) different ROI types and (C) individual patients and controls. For (B), statistical differences between the groups were assessed using the Kruskal-Wallis test, followed by post hoc pairwise comparisons using Dunn's test. For (C), statistical differences were assessed using one-way ANOVA, followed by post hoc pairwise comparisons using Tukey's HSD test. ANOVA, analysis of variance; HSD, honestly singnificant difference; ID, identification; ISG, interferon-stimulated gene; JDM, juvenile dermatomyositis; ROI, regions of interest.

S4). It is well established that both muscle and endothelium in adult and juvenile idiopathic inflammatory myopathy (IIM) express high levels of HLA class I and II proteins which can be independent of inflammatory infiltrates [17–20]. Therefore, we ascribe this result to the expression of *HLA* genes (driven by IFN) in muscle fibres or endothelium.

To determine whether differentially expressed pathways were upregulated or downregulated in JDM against controls,

gene set enrichment analysis was performed using the Fast Gene Set Enrichment Analysis (fGSEA) method [21]. This analysis provides complementary insights by considering the entire ranked gene list, identifying pathways with subtle but coordinated expression changes. Using fGSEA, 79 and 269 significant pathways (adjusted P value \leq .05, Benjamini-Hochberg procedure) were identified with the GO CC and GO BP gene sets, respectively, many of which overlapped with the ORA results.

Full lists of the significant pathways identified via fGSEA and their associated fold changes and clusters can be found in Supplementary Tables S5 (GO CC) and S6 (GO BP).

Clustering of the 79 pathways (GO CC) using aPEAR validated the previous results, with the generated network plots reinforcing involvement of ER to Golgi transport pathways (upregulated) and mitochondrial-related pathways (downregulated, Supplementary Fig S3A and Table S5). In contrast, clustering of the 269 GO BP pathways highlighted the significant upregulation of IFN signalling pathways, which fall under the cluster of 'regulation of response to external stimulus' (Supplementary Fig S3B and Table S6). Supplementary Figure S3C shows the 15 most downregulated and 15 most upregulated pathways from both GO CC and GO BP analyses, visualised by comparing normalised enrichment scores.

IFN-driven signature is elevated across tissue cell types analysed in patients with JDM

We next used our previously validated 15-gene IFN-stimulated gene signature [3] to visualise variations in the expression patterns of IFN-stimulated genes across the different ROIs, from patients and controls [22]. All 15 of these genes are associated with both type I and type II IFN signalling as annotated in the Interferome database [23]. Heatmap visualisation of normalised, scaled expression levels across ROIs revealed distinct patterns of IFN-stimulated gene (ISG) expression between patients, with unsupervised clustering of ROIs primarily by patient. One patient with JDM (JDM3) exhibited lower ISG expression compared to the other 2 patients with JDM (Fig 3A). Notably, this patient was less weak at the time of biopsy than patients JDM1 and JDM2 (Table).

Quantification of the 15-gene ISG score (IFN score) demonstrated significant elevation in all ROI types from JDM tissues compared to controls. However, pairwise comparisons using Dunn's multiple comparisons test revealed no statistically significant differences between different ROI types within the JDM group, indicating a consistent IFN activation signature across muscle cells, immune-infiltrated regions, and CD68+ macrophage-enriched regions (Fig 3B). Analysis of IFN score values by ROI confirmed that all 3 patients had significantly higher IFN scores than controls, but that the IFN score of JDM3 was significantly lower than scores of JDM1 or JDM2 (Fig 3C).

Mitochondrial dysfunction is consistent across all patients with JDM

To further analyse mitochondrial involvement within JDM muscle tissue, the 448 DEGs identified in JDM muscle ROIs compared to controls (Fig 2A) were further examined based on their associated GO terms. Of these 448 genes, 75 were annotated with the GO term 'mitochondrion'. This list was carefully curated, removing known ISGs, including 5 which were part of our IFN score, and other genes which are not specific to mitochondrial function, or only interact with mitochondria under specific conditions (see Supplementary Methods). Unsupervised clustering of the 41 remaining genes revealed clusters by ROI type (and therefore cell type), rather than by patient, suggesting that mitochondrial gene expression patterns are shaped by cell type and disease state, but were largely consistent across patients (Fig 4A). Genes included in analysis shown in Figure 4 are listed in Supplementary Table S7. Quantification of the mitochondrial gene score using these 41 genes demonstrated significant differences between all JDM ROIs and controls (Fig 4B).

Pairwise comparisons (Tukey's multiple comparisons test) revealed that among the JDM patient data, CD68 + macrophage regions exhibited significantly distinct mitochondrial scores compared to both JDM muscle (adjusted P < .0001) and control muscle ROIs (adjusted P < .0001) indicating cell-specific variation in mitochondrial gene expression patterns (Fig 4B), unlike the uniformity across cell types seen in IFN dysregulation in JDM (Fig 3B). No statistically significant difference was observed between the muscle and muscle+immune cell JDM mitochondrial scores (Fig 4B, adjusted P = .1438). Analysis of the 41-gene score across patients confirmed that each patient had a highly significant altered mitochondrial score compared to controls, but there were no significant differences in mitochondrial scores between patients (Fig 4C). Together, these results suggested that while the degree of IFN-driven pathology varied between cases, the mitochondrial abnormality was observed consistently across these 3 cases.

To validate these findings in an independent cohort, fGSEA analysis was performed using a publicly available RNAseq dataset, comparing 4 JDM with 5 control muscle biopsies [24]. As these data were bulk RNAseq, analysis was performed at the whole-biopsy level but not for specific regions or cell types within each biopsy. Analysis confirmed upregulation of IFNdriven and immune activation pathways, and downregulation of mitochondrial pathways (including oxidative phosphorylation, respiratory electron transport chain, ATP synthesis coupled electron transport), Supplementary Figure S4A. This dataset also enabled transcriptome-wide quantification, including mitochondrial-encoded gene transcripts not captured by the GeoMx whole transcriptome atlas. Of the 37 mitochondrial-encoded genes, 20 were significantly (adjusted P value <.05, $|Log2FC| \ge$ 0.58) downregulated in JDM muscle compared to controls (Supplementary Fig S4B), and this was consistent across all cases (Supplementary Fig S4C). Furthermore, 10 of the 41 mitochondrial score genes were significantly and consistently downregulated in JDM in the replication cohort (Supplementary Fig S4D, E), while 13 genes of the 15-gene IFN score were significantly upregulated in this cohort (Supplementary Fig S4F). Again, we observed clear patient heterogeneity in levels of IFN-driven gene expression (Supplementary Fig S4G).

Relationship between IFN-driven and mitochondrial abnormalities in JDM muscle

Given our intriguing finding of a lack of correlation between IFN and mitochondrial pathological gene expression, we investigated this at the protein level using conventional immunohistochemistry and chemical stains in a larger cohort (n = 19), including 16 further UK Juvenile Dermatomyositis Cohort Biomarker Study & Repository (JDCBS) JDM cases and the index 3 JDM cases, all treatment naive. Sections were stained and scored for IFN-driven MxA protein expression (Fig 5A-D) and mitochondrial abnormality (Fig 5E-J) (see Supplementary Methods). JDM cases exhibited a range of mitochondrial deficiency severity (6 severe, 10 mild, and 3 none) and IFN-driven MxA protein expression. However, there was no correlation between these 2 features (Fig 5K, P = .657). In contrast, the level of MxA protein upregulation on muscle fibres correlated with clinical weakness measured by MMT8 (adjusted P = .0369, Benjamini-Hochberg procedure) and CMAS (adjusted P = .0084), replicating our previous findings in 103 cases [25].

The histological feature of perifascicular atrophy (PFA) is well recognised in dermatomyositis and has been shown to correlate with COX deficiency and mitochondrial abnormalities in

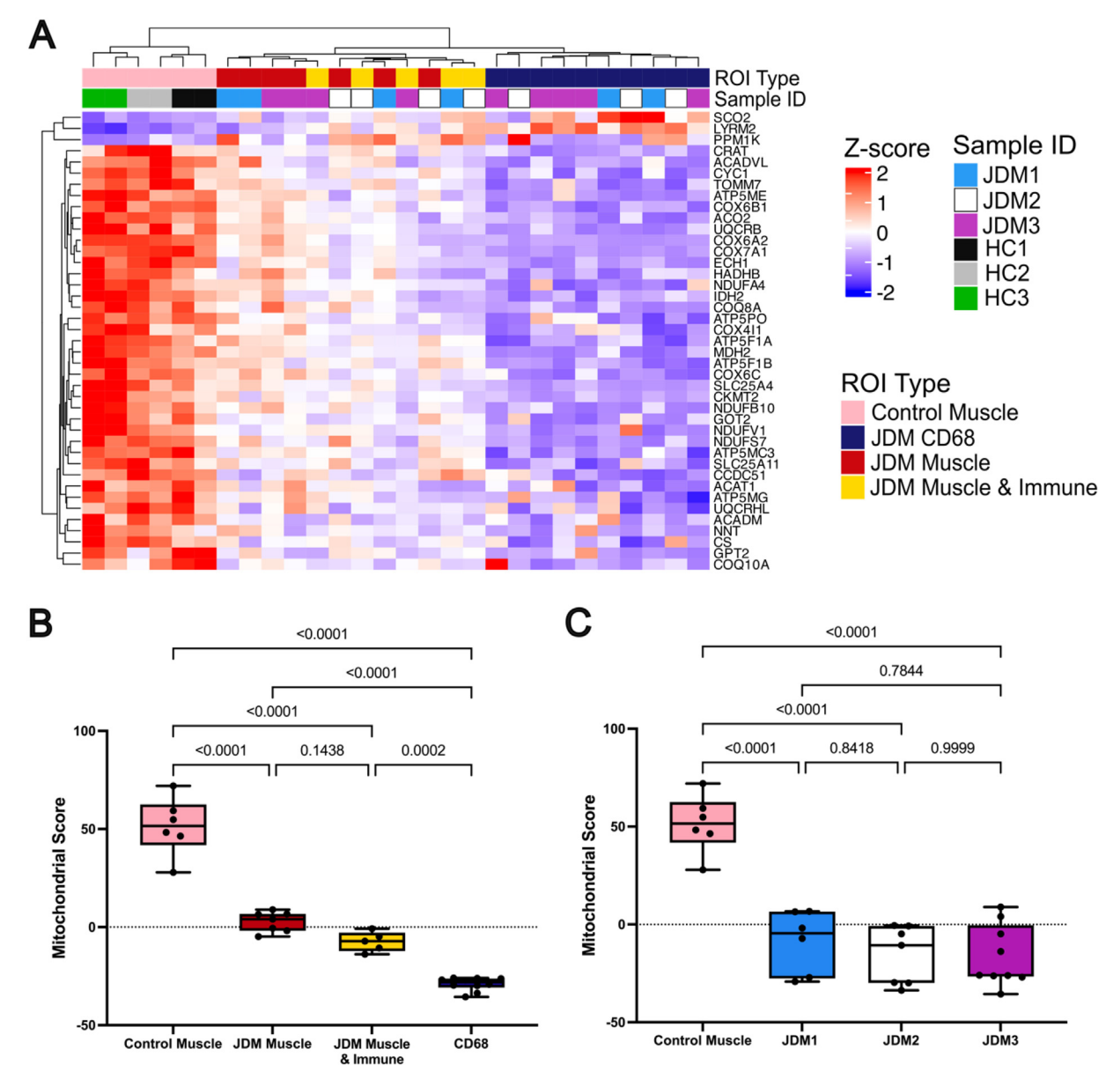


Figure 4. Abnormal mitochondrial signature is consistent across all patients with JDM but distinct between cell types. (A) Heatmap showing the normalised, scaled expression levels of the 41-gene mitochondrial score differentially expressed in JDM muscle against control ROIs. Distinct ROI types (top row) are allocated colours pink, blue, red and yellow as shown; individual patients (second row sample ID) are allocated colours as shown. All ROI types are included in the heatmap analysis. Unsupervised clustering groups the ROIs into 3 distinct clusters: one including JDM muscle ROIs and muscle + immune cell ROIs, a second for CD68 + ROIs, and a third for control muscle ROIs. The coloured scaled bar highlights the *Z*-score ranges, with red indicating a positive *Z*-score and blue indicating a negative *Z*-score. (B, C) Boxplots of 41-gene mitochondrial scores, calculated as the sum of *Z*-scores for the 41 mitochondrial genes, compared across: (B) different ROI types and (C) individual patients and controls. For (B) and (C), statistical differences were assessed using one-way ANOVA, followed by post hoc pairwise comparisons using Tukey's HSD test. ANOVA, analysis of variance; HSD, honestly significant difference; ID, identification; JDM, juvenile dermatomyositis; ROI, regions of interest.

JDM and adult DM [26]. We tested whether PFA within the ROIs analysed by GeoMx was associated with mitochondrial abnormality. All 3 JDM cases demonstrated evidence of PFA. Of the 22 ROIs, 18 contained the edge of a fascicle allowing analysis for PFA (Supplementary Fig S5A). PFA was present in 55% (10/18) of these ROI including regions from all 3 cases. In this small sample, no correlation was observed between PFA and mitochondrial abnormality, assessed in the 8 muscle/muscle + immune ROIs (Supplementary Fig S5B). However, this result may relate to small sample size, the fact that GeoMx does not measure expression of mitochondrial-encoded genes, or that each ROI covers areas with PFA and others without, while GeoMx generates a bulk-like average 41-gene mitochondrial score for the whole ROI.

To define other biological pathways associated with mitochondrial dysfunction, 2 complementary approaches were performed. First, for each pathway cluster shown in Supplementary Figure S3A, B, the most commonly shared genes within each cluster were used to generate cluster-specific expression scores. In the second approach, fGSEA was run using MSigDB Hallmark gene sets, and scores calculated from the leading-edge genes of each pathway (see Supplementary Methods). Across both methods, lower mitochondrial gene expression was consistently associated with reduced activity in metabolic pathways, including oxidative phosphorylation, fatty acid metabolism, glycolysis and genes involved in reactive oxygen species response as expected (Fig 6A, B). In addition, decreased expression of peroxisome-related genes and downregulation of sarcomere organisation

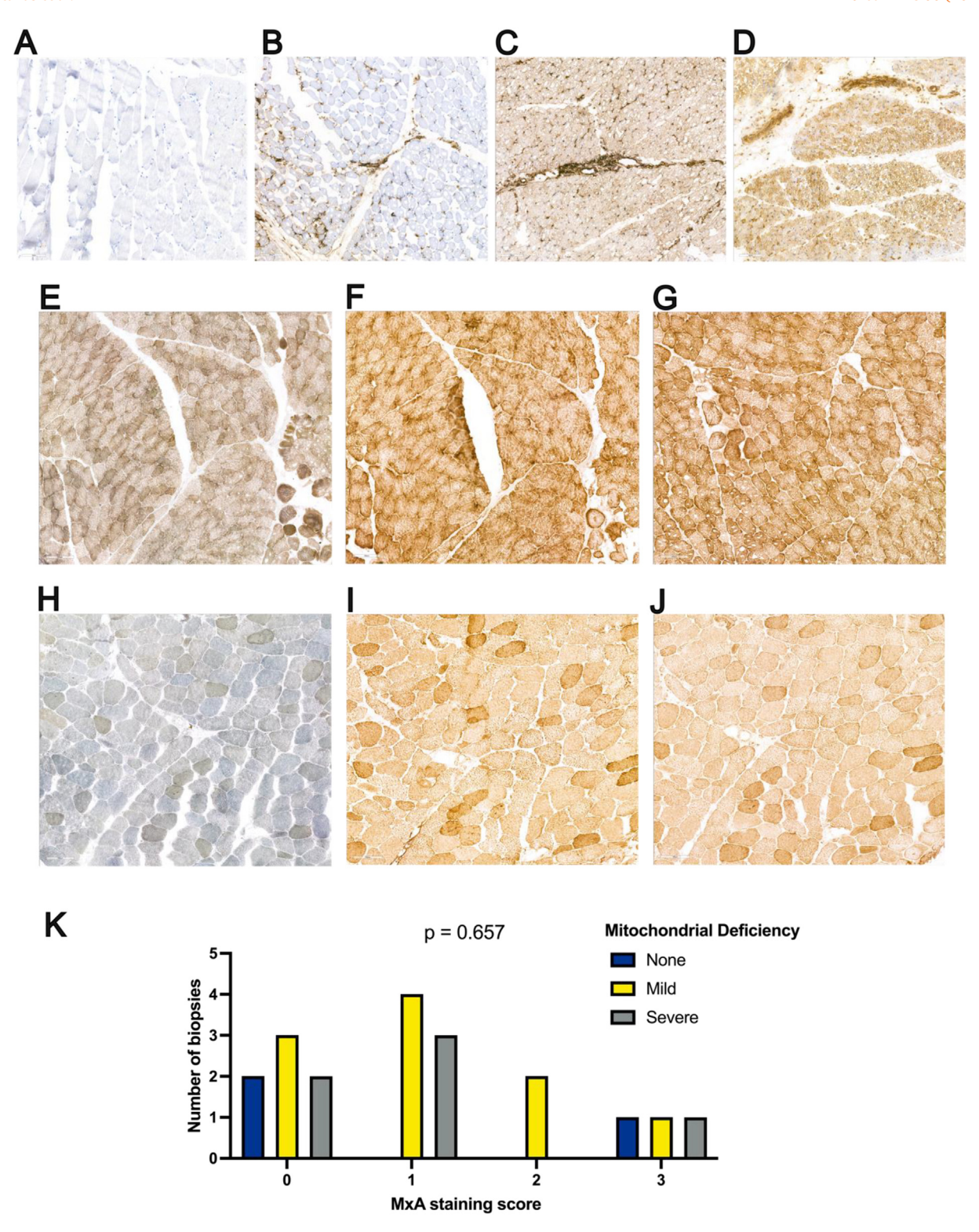


Figure 5. Lack of association between interferon dysregulation and mitochondrial deficiency assessed at protein level in an independent JDM cohort. (A-D) Representative immunohistochemical staining for myxovirus-resistance protein A (MxA), used to assess interferon-driven protein expression in muscle fibres. Scoring was performed using a 4-point scale: 0 = no staining (A), 1 = weak (B), 2 = moderate (C), and 3 = strong (D). (E-J) Representative staining for mitochondrial deficiency, assessed using combined COX—SDH histochemistry and supported by immunohistochemistry for MTCO1 (complex IV) and NDUFB8 (complex I). Cases were categorised as having no (0), mild (1), or severe (2) mitochondrial deficiency. (E-G) Representative staining from a JDM biopsy with mild mitochondrial deficiency: (E) COX—SDH staining, (F) MTCO1, and (G) NDUFB8. (H-J) Representative staining from a JDM biopsy with severe mitochondrial deficiency: (H) COX—SDH, (I) MTCO1, and (J) NDUFB8. (K) Summary bar plot of 19 JDM muscle biopsies, showing the distribution of mitochondrial deficiency scores (0 = none, 1 = mild, 2 = severe) across each level of interferon activity (MxA score 0–3). Bar colours indicate the level of mitochondrial deficiency (none, mild, severe) as shown. Statistical analysis was performed using the *U*-statistic permutation test. JDM, juvenile dermatomyositis.

A.E. Syntakas et al. Ann Rheum Dis 00 (2025) 1–15

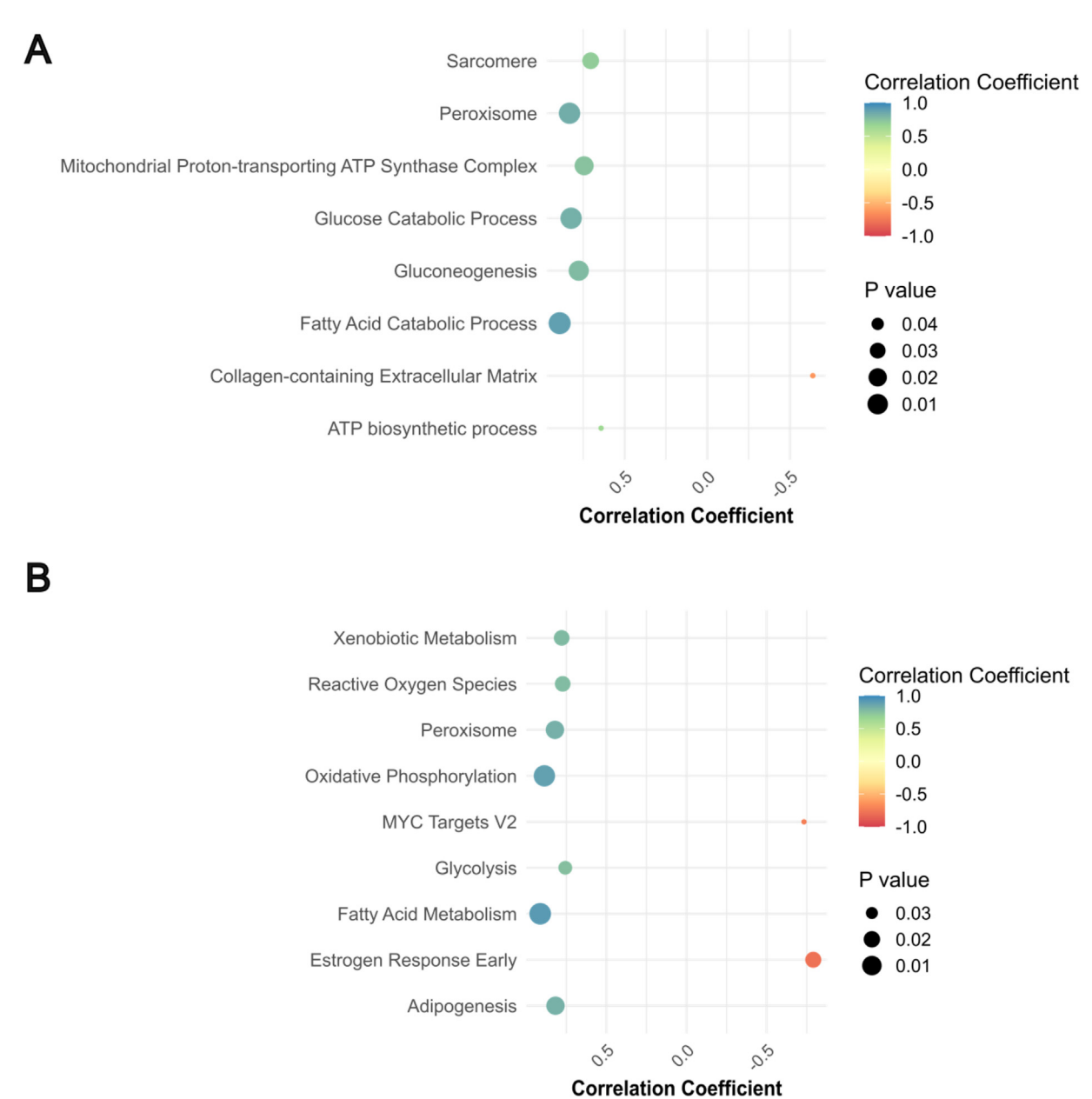


Figure 6. Pathway-level transcriptional signatures associated with mitochondrial dysfunction in JDM muscle. Dot plots show the significant correlation between the mitochondrial gene score and pathway-specific expression scores across muscle regions of interest (ROIs) from JDM biopsies (adjusted $P \le .05$, Benjamini-Hochberg procedure). The mitochondrial gene score was calculated per ROI based on *z*-scores of 41 curated mitochondrial genes, using the mean and SD from control muscle as a reference. (A) Correlation with GO-based pathway clusters, derived from fGSEA of JDM ROIs compared to controls. For each cluster, a core gene signature was defined by selecting genes that appeared in the leading edge of ≥75% of constituent pathways. (B) Correlation with significantly enriched MSigDB Hallmark pathways (adjusted $P \le .05$, Benjamini-Hochberg procedure) identified through gene set enrichment analysis of JDM vs control muscle. For both (A) and (B), each dot represents a single pathway or cluster. Dot size reflects the strength of the correlation (r coefficient), and dot colour indicates the statistical significance of the correlation, with deeper red shades corresponding to smaller adjusted P values. The colour scale bar reflects the adjusted P value. GO, gene ontology; JDM, juvenile dermatomyositis.

were observed to be correlated with more severe mitochondrial abnormalities.

Transcriptomic differences between distinct regions of affected muscle and between patients

Since we observed differences in IFN-driven signature between cases, we tested for other transcriptomic differences across patients, comparing patient JDM3 with JDM1 and JDM2. Initially, muscle and muscle-immune ROIs were combined to increase statistical power. Analysis comparing JDM3 vs JDM1 + JDM2 revealed 176 DEGs between groups (100 upregulated, 76 downregulated genes in patients JDM1+JDM2,

Supplementary Fig S6A). Pathway analysis indicated 208 enriched GO BP pathways; cluster network analysis highlighted IFN and immune-related pathway clusters, including 'positive regulation of type I interferon production' (confirming our 15-gene IFN score result, Fig 3), 'antigen processing and presentation via MHC Class I via ER pathways', and 'antibacterial humoral response' (Supplementary Fig S6B). In this comparison between patients, mitochondrial pathways were not differentially expressed, confirming earlier results suggesting consistent mitochondrial abnormalities in all cases. Separate DGE analysis performed between the CD68+ cell ROIs of patient JDM3 against those of patients JDM1+JDM2 revealed 63 DEGs (43 upregulated, 20 downregulated in JDM1+JDM2,

A.E. Syntakas et al. Ann Rheum Dis 00 (2025) 1–15

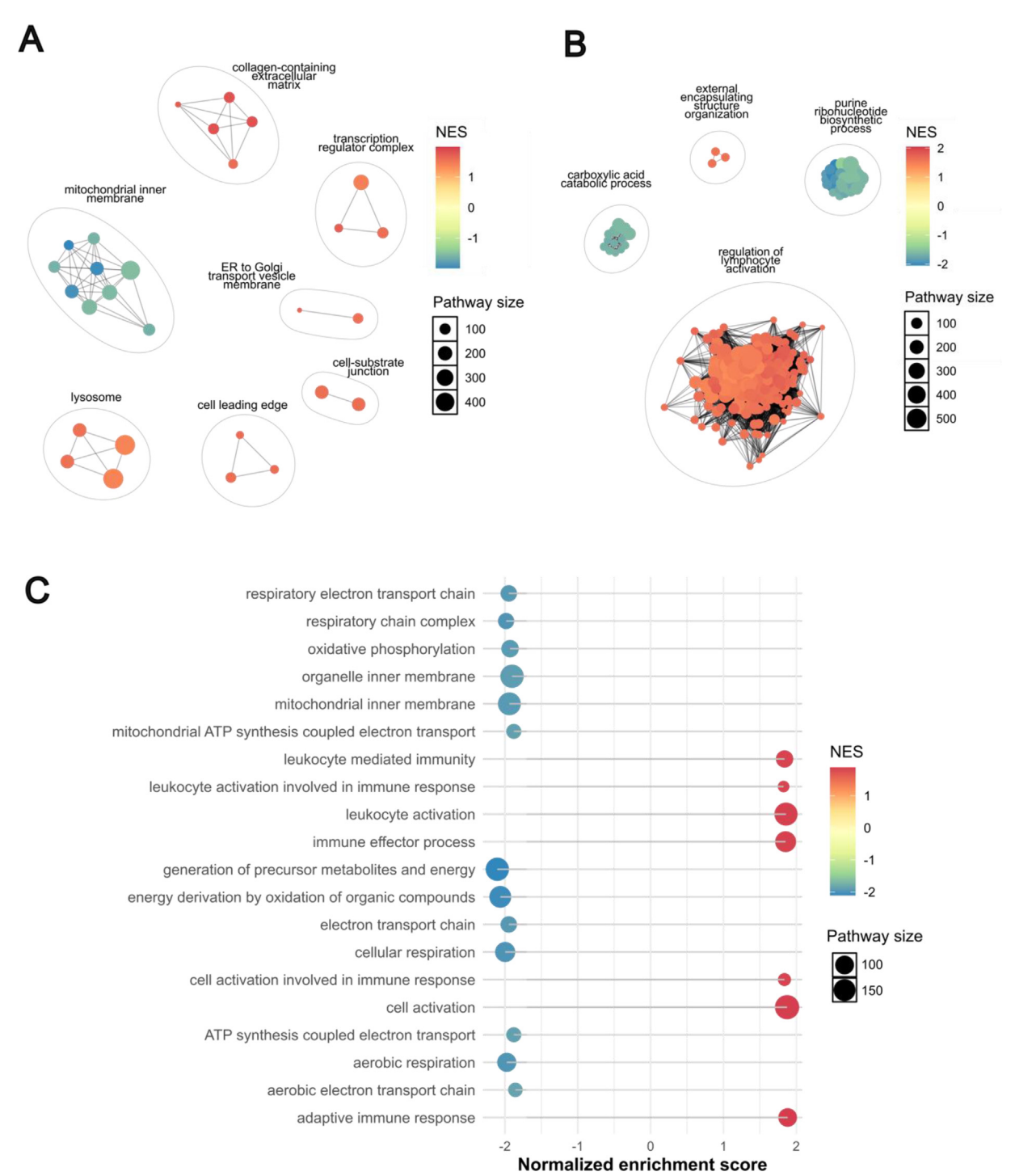


Figure 7. Gene set enrichment analysis reveals increased immune pathways and decreased mitochondrial functional pathways in JDM immune cell-rich muscle regions compared to JDM muscle-only regions. (A, B) Cluster plots of enriched gene ontology pathways, based on fGSEA performed on all genes for each comparison ranked by *P* value and fold change. (A) Plot of enriched GO cellular component pathways. (B) Plot of enriched GO biological process pathways. (C) Dot plot of the 20 GO BP and CC pathways with the highest absolute normalised enrichment score (NES). In panels (A-C), larger dots represent pathways associated with a higher number of genes (shown in key, pathway size), and the dot colour reflects the NES, with blue indicating negative NES and red indicating positive (shown in colour bar, NES). BP, biological process; CC, cellular component; GO, gene ontology; JDM, juvenile dermatomyositis.

Supplementary Fig S7A). Within this analysis, 148 GO BP pathways were significantly enriched, with the most prominent cluster being 'negative regulation of viral genome replication' (Fig 7B), indicating that expression of ISGs in muscle-infiltrating CD68+ cells also differed between the patients with JDM. We also conducted DGE analysis for each ROI type comparing JDM1+JDM3 vs JDM2, and JDM2+JDM3 vs JDM1. Those comparisons did not reveal meaningful differences, yielding between 0 and 4 DEGs only (data not shown).

Finally, we explored transcriptional patterns in muscle-immune ROI (which had dense infiltrates of CD45+ immune cells, including CD3+/CD68+/CD20+ cells), compared to muscle-fibre only regions. Initial DGE analysis using the limma-voom pipeline suggested no significant DEGs between these ROI groups, based on the same fold change and adjusted *P* value criteria (data not shown). However, fGSEA analysis revealed 28 significant pathways in the GO CC gene set and 317 significant pathways in the GO BP gene set (Fig 7A, B,

respectively). These pathway-level findings suggested that immune-infiltrated muscle regions exhibited further downregulation of mitochondrial and metabolic pathways, alongside increased expression of immune-related and leukocyte activation pathways (Fig 7C). While not captured at the significant DEG level, these transcriptional differences are consistent with the expected biological impact of immune infiltration. These significant pathways are found in Supplementary Tables S8 (GO CC) and S9 (GO BP).

DISCUSSION

Our previous work and that of others studying affected muscle in JDM, a key target tissue of pathology, has demonstrated upregulated expression of IFN-driven gene and protein expression. In muscle fibres, this includes overexpression of class I MHC protein (also known as HLA class I) [6,20,27], and myxovirus-resistance protein A [25]. Expression of IFN-driven proteins is variable between cases, but typically correlates with the degree of weakness [25]. Many studies have confirmed a strong IFN-driven transcriptional signature in both muscle and blood of both adult and paediatric patients with IIM [3,28–31]. Therapies which target IFN or IFN signalling are increasingly being tested in myositis [32].

Our previous gene expression analysis of peripheral blood lineage-sorted immune cells from patients with JDM revealed not only this known IFN-driven signature, but also a signature of mitochondrial dysfunction, most marked in blood monocytes [3] which was confirmed at the functional level and found to persist, and was not restored to normal by treatment, despite clear reduction in expression of ISGs on treatment. Furthermore, we showed that mitochondrial DNA was abnormally released in patient monocytes and could drive production of IFN and downstream ISGs, an effect that was mediated via C-GAS-STING and TLR9 pathways.

To date, the majority of transcriptional studies published using muscle tissue of patients with IIM have used bulk RNA sequencing. In these datasets, it is challenging to understand or define the role of different cells, or to identify how specific tissue microniches contribute to pathology. In this study, we have for the first time used spatial transcriptomic methods to analyse muscle tissue from children with JDM obtained at diagnosis before starting treatment compared to age-matched healthy muscle. Thus, our data are not confounded by the effects of medication. We used Nanostring GeoMx DSP to generate transcriptional data of 3 specific region types within the muscle. This allowed comparison of regions within the disease tissue including those where infiltrating immune cells are scarce, or not detected, in regions of dense clusters of inflammatory cells, and in regions where CD68+ infiltrating macrophages were predominant. Our data confirm successful use of this platform for analysis using historical cryopreserved muscle tissue.

Initial analysis of JDM compared to control tissue confirmed high expression of IFN-stimulated genes in all regions analysed. Furthermore, strong upregulation of pathways related to protein transport through the ER and Golgi, and ER stress, was observed, aligning well with our previous studies in human muscle and a transgenic mouse myositis model [4,33,34]. We also demonstrate that, as previously observed in blood monocytes, in the JDM tissue itself, muscle fibres have a highly dysregulated mitochondrial signature. Dysregulated pathways included those related to mitochondrial function, respiratory chain, and mitochondrial proton transport: their expression was downregulated in muscle. In addition, the signal for mitochondrial and

respiratory chain-related genes was distinct in CD68-enriched regions. By analysing RNAseq data from a second JDM cohort, we validated our results for these nuclear-encoded mitochondrial genes and additionally showed downregulation of mitochondrial-encoded genes. We investigated the relationship of the signatures to clinical activity as assessed by muscle weakness. We observed a correlation between IFN signature and weakness, whereby 1 patient who was minimally weak (MMT8 score 78) had lower expression of IFN-induced signature than the 2 patients who were significantly weak (MMT8 scores 44 and 42). Interestingly, this was different for the mitochondrial signature detected in tissue, which was independent of the IFN signature. The downregulation of mitochondrial pathways was consistently observed for the index 3 patients, regardless of muscle strength, and across the 3 patients this result showed minimal variance for the 41-gene mitochondrial score we defined. We extended these findings in 19 cases at protein level, and replicated the observation of no correlation between level of IFNdriven protein expression with mitochondrial abnormality. A recent study suggested that IFNg itself leads to mitochondrial dysfunction and oxidative stress in both a mouse model and patients with adult IIM [10]. In contrast, our previous work in JDM monocytes suggested that circulating oxidised mitochondrial DNA itself may activate IFN pathways. The current study suggests that mitochondrial dysfunction can be equally prominent in patients with either low or high IFN score at both RNA and protein level, implying that IFN-independent drivers of mitochondrial dysfunction exist. If so, blocking of IFN by new therapeutic agents may not adequately control all aspects of disease pathology. Supporting this, recent evidence in Inclusion Body Myositis (IBM) and Polymyositis (PM) suggests that mitochondrial-encoded gene mutations lead to inflammation and immune cell infiltration, activating the cGAS/STING pathway, in the absence of IFN [35]. In a model of Parkinson's disease (PD) and patients with PD, mitochondrial DNA damage triggers neuron pathology, which is, remarkably, exacerbated in the IFN-deficient mouse [36]. Collectively, these findings suggest that the intersection between mitochondrial biology and IFN is bidirectional and complex, and that pathologies driven by altered mitochondrial DNA and function can act independently of IFN. Our demonstration that mitochondrial dysfunction correlates with altered function of the peroxisome, an organelle key to metabolic pathways which communicates with mitochondria, may reveal further potential novel treatment targets [37].

Our analysis of JDM muscle compared to healthy muscle also revealed other dysregulated pathways associated with disease, including ER to Golgi transport, sarcomere and T cell activation. We attribute this to the highly upregulated HLA class I and II DEGs which are known to be upregulated in muscle fibres themselves in JDM.

Direct comparison of muscle-only to muscle+immune regions revealed pronounced downregulation of mitochondrial and metabolic pathways, alongside increased expression of immune-related pathways, in immune-infiltrated regions. This indicates that relative mitochondrial abnormalities differ between cell types in inflamed tissue, and concurs with evidence that the mitochondrial transcriptome differs across tissue types [38]. To precisely dissect specific tissue niches and cell interactions in JDM, future single-cell spatial analyses will provide a more precise understanding of cell-specific contributions and define cell-cell interactions in JDM muscle tissue. Single-cell spatial analysis of JDM muscle is underway to allow us to distinguish these issues.

This study has several limitations. The initial sample size (n = 3 in each group) was small which limited our ability to

detect gene expression differences with a small effect size, which may still be important to pathology: therefore, our findings should be interpreted with caution, especially when comparing 2 patients to one other. In addition, the 3 initial JDM and 3 control cases are not perfectly matched for sex or age, and in this group size it was not possible to adjust for these variables. Thus, despite close clustering of the control case data in both PCA and gene score analyses, larger studies are needed to assess the effect of these variables on muscle transcription in myositis.

Despite this, key significant differences between patients and controls were replicated in a second cohort and our findings were validated at protein level in a larger cohort. Our previous analysis of 103 JDM muscle biopsies showed significant histological heterogeneity across cases which varied in part by MSA status [25]. The current study was not powered to analyse for association between specific MSA status and transcriptional differences. A larger cohort will therefore be essential to capture the full variance in patient phenotype, MSA status, clinical severity, and pathology, to provide a robust understanding of JDM-associated gene expression changes. Furthermore, analysis of tissue-infiltrating CD68+ macrophages lacked a control comparison group due to the absence of CD68+ cells in normal muscle tissue limiting our ability to identify the unique transcriptomic signature of infiltrating macrophages against healthy macrophages.

This study represents the first application of spatial transcriptomics to muscle biopsies from a patient with JDM using the GeoMx technology, unveiling critical insights into mitochondrial and immune dysregulation at the tissue level. Importantly, we have defined parallel gene expression patterns in both the muscle and macrophage-rich regions of JDM muscle, as previously identified in blood monocytes. Together, these data suggest that mitochondrial dysfunction is present across tissues and, that within the muscle itself, this signal is readily detectable in both CD68+ infiltrating cells and muscle fibres. Our results also indicate that this mitochondrial dysfunction is uncoupled from the characteristic IFN-driven signature. Given that almost 50% of patients with JDM are not well-controlled on standard first-line treatments [2], which are currently focused on the suppression of immune pathways, our demonstration that mitochondrial dysfunction is present in the muscle of the majority of cases of JDM in this study has important implications. First, adjunctive therapies that target the mitochondrial pathology could be tested in combination with current treatments. Second, this signature may be readily tested and used to drive treatment choices in the future. Future work to define whether the mitochondrial signature in tissue correlates with that in blood will be important for the design of stratification tools in trials of novel agents targeting the mitochondrial abnor-

Our findings advance the understanding of JDM pathogenesis and lay the groundwork for future research into the use of therapies which specifically target mitochondrial dysfunction and immune-mediated damage.

Competing interests

LRW reports financial support was provided by Versus Arthritis, UK Research and Innovation Medical Research Council, National Institute for Health and Care Research, Myositis UK, Great Ormond Street Hospital Children's Charity, and Cure JM Foundation. MGLW reports financial support was provided by Versus Arthritis, National Institute for Health and Care Research, Connect Immune Partnership, Myositis UK, and Great

Ormond Street Hospital Children's Charity. APC reports financial support was provided by The Kennedy Trust for Rheumatology Research. LRW reports a relationship with Pfizer Inc that includes: consulting or advisory, funding grants, and speaking and lecture fees. LRW reports a relationship with Cabaletta Bio Inc that includes: consulting or advisory. LRW reports a relationship with Eli Lilly and Company that includes: funding grants. The other authors declare they have no competing interests.

CRediT authorship contribution statement

Aris E. Syntakas: Writing - original draft, Visualization, Software, Methodology, Investigation, Formal analysis, Data curation. Melissa Kartawinata: Writing - review & editing, Methodology, Data curation. Nia M.L. Evans: Writing – review & editing, Methodology, Data curation. Huong D. Nguyen: Writing - review & editing, Methodology, Data curation. Charalampia Papadopoulou: Writing - review & editing, Data curation. Muthana Al Obaidi: Writing – review & editing, Data curation. Clarissa Pilkington: Writing - review & editing, Data curation. Yvonne Glackin: Writing - review & editing, Data curation. **Christopher B. Mahony:** Writing – review & editing, Formal analysis. Adam P. Croft: Writing - review & editing, Formal analysis. **Simon Eaton:** Writing – review & editing, Formal analysis. **Mario Cortina-Borja:** Writing – review & editing, Methodology, Data curation. Olumide Ogunbiyi: Writing review & editing, Visualization, Software, Investigation. Ashirwad Merve: Writing - review & editing, Visualization, Software, Investigation. Lucy R. Wedderburn: Writing – review & editing, Writing - original draft, Supervision, Resources, Project administration, Methodology, Funding acquisition, Formal analysis, Conceptualization. Meredyth G. Ll Wilkinson: Writing review & editing, Writing – original draft, Supervision, Resources, Project administration, Methodology, Funding acquisition, Formal analysis, Conceptualization.

Patient and public involvement and engagement

Patients and carers were involved at every stage of this research, including study conception, design, delivery, and analysis, through our partnership stakeholder group, the JDCBS PPIE group. The study was discussed at our annual JDCBS study day and also at the UK JDM Family Day, where families, patients, and parents provided input. All patients and families who are part of the study across the UK hear about updates via a regular newsletter as well as on our dedicated website.

Acknowledgements

We thank all of the families, patients, parents, and carers who contributed to the study and allowed us to use samples and data for this work. We are very grateful to Mr Dario Cancemi for excellent study management, to the clinical team who assist with data collection, to Dr Lizzy Rosser for critical review and to the BRAIN Bank UK for access to control cases. We are grateful to the members of the JDCBS research group (JDRG) and who are listed in the supplementary materials. We thank the team at Nanostring for valuable guidance, the GOSH histopathology team including Abigail White and Mwaka Mshanga, and Darren Chambers, Department of Neuropathology, UCL Queen Square Institute of Neurology for chemical stains. We thank Mr J A McBride for advice on colour figures.

The data presented in this manuscript have not been published previously. However, some of the data were submitted as

A.E. Syntakas et al.

an abstract for the European Alliance of Associations for Rheumatology (EULAR) 2025 congress.

Contributors

AES contributed to data curation, led the development of the formal analysis and methodology pipeline, visualisation, and drafting of the original manuscript. MK, HDN, NMLE and MC-B contributed to data curation and methodology development. APC, CBM and SE contributed to analysis. ChP, MAO, ClP and YG contributed to data collection and curation. AM and OO were responsible for histopathology analysis. LRW and MGLW conceptualised the study, acquired funding and coled analysis, methodology development, project supervision. LRW, MGLW and MK contributed to both original drafting and editing of the manuscript. All authors reviewed and approved the final manuscript for submission.

Funding

This study was supported by generous grants from Versus Arthritis (Career Development fellowship to MLGW ref 23202, and PhD studentship to AS, ref 23202, Centre grant ref 21593 to LRW), Myositis UK, Great Ormond Street Children's Charity (W1143, and W1183), NIHR Biomedical Research Centre at GOSH (fellowship to MW ref 18IR33) and the Connect Immune Partnership (ref 22936). The work was also supported by grants from the Medical Research Council (MR/N003322/1 and MR/R013926/1), and Cure JM. APC is funded by a Kennedy Trust for Rheumatology Research Senior Fellowship KENN 19 20 06.

Patient consent for publication

Not applicable, consent provided through recruitment to ethically approved study.

Ethics approval

This study involves human participants; the study was fully approved by the North-East Yorkshire Research Ethics Committee (MREC 01/3/022). All participants gave fully informed consent (or had parental fully informed consent), and age-appropriate assent, in accordance with the declaration of Helsinki.

Provenance and peer review

Not commisioned; externally peer reviewed.

Data availability statement

The data that support the findings of this study are available from the corresponding authors on reasonable request. Script used in analyses is openly available in GitHub (https://github.com/WedderburnLab/GeoMx-pipeline).

Supplementary materials

Supplementary material associated with this article can be found in the online version at doi:10.1016/j.ard.2025.07.015.

Orcid

Aris E. Syntakas: http://orcid.org/0009-0004-6225-9373 Melissa Kartawinata: http://orcid.org/0000-0002-9432-393X Nia M.L. Evans: http://orcid.org/0009-0004-9922-8896 Huong D. Nguyen: http://orcid.org/0000-0003-1524-8028 Charalampia Papadopoulou: http://orcid.org/0000-0002-1237-0557

Muthana Al Obaidi: http://orcid.org/0000-0002-2144-3682 Clarissa Pilkington: http://orcid.org/0000-0003-2289-2428 Christopher B. Mahony: http://orcid.org/0000-0003-4487-2540

Adam P. Croft: http://orcid.org/0000-0002-9487-0511 Simon Eaton: http://orcid.org/0000-0003-0892-9204 Mario Cortina-Borja: http://orcid.org/0000-0003-0627-2624 Olumide Ogunbiyi: http://orcid.org/0000-0001-5208-5526 Ashirwad Merve: http://orcid.org/0000-0001-9715-1849 Lucy R. Wedderburn: http://orcid.org/0000-0002-7495-20

Meredyth G. Ll Wilkinson: http://orcid.org/0000-0002-7972-8066

REFERENCES

- [1] Kim H. Updates on interferon in juvenile dermatomyositis: pathogenesis and therapy. Curr Opin Rheumatol 2021;33(5):371–7. doi: 10.1097/ BOR.000000000000000816.
- [2] Papadopoulou C, Chew C, Wilkinson MGL, McCann L, Wedderburn LR. Juvenile idiopathic inflammatory myositis: an update on pathophysiology and clinical care. Nat Rev Rheumatol 2023;19(6):343–62. doi: 10.1038/s41584-023-00967-9.
- [3] Wilkinson MGL, Moulding D, McDonnell TCR, Orford M, Wincup C, Ting JYJ, et al. Role of CD14+ monocyte-derived oxidised mitochondrial DNA in the inflammatory interferon type 1 signature in juvenile dermatomyositis. Ann Rheum Dis 2023;82(5):658–69. doi: 10.1136/ard-2022-223469.
- [4] Nistala K, Varsani H, Wittkowski H, Vogl T, Krol P, Shah V, et al. Myeloid related protein induces muscle derived inflammatory mediators in juvenile dermatomyositis. Arthritis Res Ther 2013;15(5):R131. doi: 10.1186/ar4311.
- [5] Yasin SA, Schutz PW, Deakin CT, Sag E, Varsani H, Simou S, et al. Histological heterogeneity in a large clinical cohort of juvenile idiopathic inflammatory myopathy: analysis by myositis autoantibody and pathological features. Neuropathol Appl Neurobiol 2019;45(5):495–512. doi: 10.1111/nan.12528.
- [6] Varsani H, Charman SC, Li CK, Marie SKN, Amato AA, Banwell B, et al. Validation of a score tool for measurement of histological severity in juvenile dermatomyositis and association with clinical severity of disease. Ann Rheum Dis 2015;74(1):204–10. doi: 10.1136/annrheumdis-2013-203396.
- [7] Arnold L, Henry A, Poron F, Baba-Amer Y, van Rooijen N, Plonquet A, et al. Inflammatory monocytes recruited after skeletal muscle injury switch into antiinflammatory macrophages to support myogenesis. J Exp Med 2007;204 (5):1057–69. doi: 10.1084/jem.20070075.
- [8] Hernandez-Torres F, Matias-Valiente L, Alzas-Gomez V, Aranega AE. Macrophages in the context of muscle regeneration and duchenne muscular dystrophy. Int J Mol Sci 2024;25(19):10393.
- [9] Li Z, Liu H, Xie Q, Yin G. Macrophage involvement in idiopathic inflammatory myopathy: pathogenic mechanisms and therapeutic prospects. J Inflamm (Lond) 2024;21(1):48. doi: 10.1186/s12950-024-00422-w.
- [10] Abad C, Pinal-Fernandez I, Guillou C, Bourdenet G, Drouot L, Cosette P, et al. IFN γ causes mitochondrial dysfunction and oxidative stress in myositis. Nat Commun 2024;15(1):5403. doi: 10.1038/s41467-024-49460-1.
- [11] Piñeiro AJ, Houser AE, Ji AL. Research techniques made simple: spatial transcriptomics. J Invest Dermatol 2022;142(4):993–1001.e1. doi: 10.1016/j.jid.2021.12.014.
- [12] Böning S, Schneider F, Huber AK, Langhoff D, Lin H, Kaczorowski A, et al. Region of interest localization, tissue storage time, and antibody binding density-a technical note on the GeoMx® Digital Spatial Profiler. Immunooncol Technol 2024;23:100727. doi: 10.1016/j.iotech.2024.100727.
- [13] Lam CG, Manlhiot C, Pullenayegum EM, Feldman BM. Efficacy of intravenous Ig therapy in juvenile dermatomyositis. Ann Rheum Dis 2011;70(12):2089– 94. doi: 10.1136/ard.2011.153718.
- [14] Varsani H, Newton KR, Li CK, Harding B, Holton JL, Wedderburn LR. Quantification of normal range of inflammatory changes in morphologically normal pediatric muscle. Muscle Nerve 2008;37(2):259–61. doi: 10.1002/mus.20898.
- [15] Law CW, Chen Y, Shi W, Smyth GK. voom: precision weights unlock linear model analysis tools for RNA-seq read counts. Genome Biol 2014;15(2):R29. doi: 10.1186/gb-2014-15-2-r29.

[16] Kerseviciute I, Gordevicius J. aPEAR: an R package for autonomous visualization of pathway enrichment networks. Bioinformatics 2023;39(11):btad672. doi: 10.1093/bioinformatics/btad672.

- [17] Emslie-Smith AM, Arahata K, Engel AG. Major histocompatibility complex class I antigen expression, immunolocalization of interferon subtypes, and T cell-mediated cytotoxicity in myopathies. Hum Pathol 1989;20(3):224–31. doi: 10.1016/0046-8177(89)90128-7.
- [18] Englund P, Lindroos E, Nennesmo I, Klareskog L, Lundberg IE. Skeletal muscle fibers express major histocompatibility complex class II antigens independently of inflammatory infiltrates in inflammatory myopathies. Am J Pathol 2001;159(4):1263–73. doi: 10.1016/S0002-9440(10)62513-8.
- [19] Englund P, Nennesmo I, Klareskog L, Lundberg IE. Interleukin-1alpha expression in capillaries and major histocompatibility complex class I expression in type II muscle fibers from polymyositis and dermatomyositis patients: important pathogenic features independent of inflammatory cell clusters in muscle tissue. Arthritis Rheum 2002;46(4):1044–55. doi: 10.1002/art.10140.
- [20] Li CK, Varsani H, Holton JL, Gao B, Woo P, Wedderburn LR, et al. MHC class I overexpression on muscles in early juvenile dermatomyositis. J Rheumatol 2004;31(3):605–9.
- [21] Korotkevich G, Sukhov V, Budin N, Shpak B, Artyomov MN, Sergushichev A. Fast gene set enrichment analysis. bioRxiv 2021:060012. doi: 10.1101/060012.
- [22] Gu Z, Eils R, Schlesner M. Complex heatmaps reveal patterns and correlations in multidimensional genomic data. Bioinformatics 2016;32(18):2847–9. doi: 10.1093/bioinformatics/btw313.
- [23] Rusinova I, Forster S, Yu S, Kannan A, Masse M, Cumming H, et al. INTER-FEROME v2.0: an updated database of annotated interferon-regulated genes. Nucleic Acids Res 2013;41:D1040–6 (Database issue). doi: 10.1093/nar/gks1215.
- [24] Roberson EDO, Mesa RA, Morgan GA, Cao L, Marin W, Pachman LM. Transcriptomes of peripheral blood mononuclear cells from juvenile dermatomyositis patients show elevated inflammation even when clinically inactive. Sci Rep 2022;12(1):275. doi: 10.1038/s41598-021-04302-8.
- [25] Soponkanaporn S, Deakin CT, Schutz PW, Marshall LR, Yasin SA, Johnson CM, et al. Expression of myxovirus-resistance protein A: a possible marker of muscle disease activity and autoantibody specificities in juvenile dermatomy-ositis. Neuropathol Appl Neurobiol 2019;45(4):410–20. doi: 10.1111/nan.12498.
- [26] Hedberg-Oldfors C, Lindgren U, Visuttijai K, Lööf D, Roos S, Thomsen C, et al. Respiratory chain dysfunction in perifascicular muscle fibres in patients with dermatomyositis is associated with mitochondrial DNA depletion. Neuropathol Appl Neurobiol 2022;48(7):e12841. doi: 10.1111/nan.12841.
- [27] Wedderburn LR, Varsani H, Li CK, Newton KR, Amato AA, Banwell B, et al. International consensus on a proposed score system for muscle

- biopsy evaluation in patients with juvenile dermatomyositis: a tool for potential use in clinical trials. Arthritis Rheum 2007;57(7):1192–201. doi: 10.1002/art.23012.
- [28] Pinal-Fernandez I, Casal-Dominguez M, Derfoul A, Pak K, Plotz P, Miller FW, et al. Identification of distinctive interferon gene signatures in different types of myositis. Neurology 2019;93(12):e1193–204. doi: 10.1212/WNL.00000 00000008128.
- [29] Corman VM, Preusse C, Melchert J, Melchert J, Benveniste O, Koll R, et al. Deep RNA sequencing of muscle tissue reveals absence of viral signatures in dermatomyositis. Free Neuropathol 2024;5:1. doi: 10.17879/freeneuropathology-2024-5149.
- [30] Bilgic H, Ytterberg SR, Amin S, McNallan KT, Wilson JC, Koeuth T, et al. Interleukin-6 and type I interferon-regulated genes and chemokines mark disease activity in dermatomyositis. Arthritis Rheum 2009;60(11):3436–46. doi: 10.1002/art.24936.
- [31] Baechler EC, Bauer JW, Slattery CA, Ortmann WA, Espe KJ, Novitzke J, et al. An interferon signature in the peripheral blood of dermatomyositis patients is associated with disease activity. Mol Med 2007;13(1-2):59–68. doi: 10.2119/2006-00085.Baechler.
- [32] Ll Wilkinson MG, Deakin CT, Papadopoulou C, Eleftheriou D, Wedderburn LR. JAK inhibitors: a potential treatment for JDM in the context of the role of interferon-driven pathology. Pediatr Rheumatol Online J 2021;19(1):146. doi: 10.1186/s12969-021-00637-8.
- [33] Rayavarapu S, Coley W, Nagaraju K. Endoplasmic reticulum stress in skeletal muscle homeostasis and disease. Curr Rheumatol Rep 2012;14(3):238–43. doi: 10.1007/s11926-012-0247-5.
- [34] Li CK, Knopp P, Moncrieffe H, Singh B, Shah S, Nagaraju K, et al. Overexpression of MHC class I heavy chain protein in young skeletal muscle leads to severe myositis: implications for juvenile myositis. Am J Pathol 2009;175 (3):1030–40. doi: 10.2353/ajpath.2009.090196.
- [35] Kleefeld F, Cross E, Lagos D, Walli S, Schoser B, Hentschel A, et al. Mitochondrial damage is associated with an early immune response in inclusion body myositis. Brain 2025:awaf118. doi: 10.1093/brain/awaf118.
- [36] Tresse E, Marturia-Navarro J, Sew WQG, Cisquella-Serra M, Jaberi E, Riera-Ponsati L, et al. Mitochondrial DNA damage triggers spread of Parkinson's disease-like pathology. Mol Psychiatry 2023;28(11):4902–14. doi: 10.1038/s41380-023-02251-4.
- [37] Picca A, Faitg J, Auwerx J, Ferrucci L, D'Amico D. Mitophagy in human health, ageing and disease. Nat Metab 2023;5(12):2047–61. doi: 10.1038/ s42255-023-00930-8.
- [38] Ali AT, Boehme L, Carbajosa G, Seitan VC, Small KS, Hodgkinson A. Nuclear genetic regulation of the human mitochondrial transcriptome. Elife 2019;8: e41927. doi: 10.7554/eLife.41927.